

**Inelastic low-energy electron collisions with the HBr and DBr molecules: Experiment and theory**

M. Čížek and J. Horáček

*Department of Theoretical Physics, Faculty of Mathematics and Physics, Charles University Prague, V Holešovičkách 2, 180 00 Praha 8, Czech Republic*

A.-Ch. Sergenton, D. B. Popović, and M. Allan

*Institute of Physical Chemistry, University of Fribourg, Pérolles, 1700 Fribourg, Switzerland*

W. Domcke

*Institute of Physical and Theoretical Chemistry, Technical University of Munich, D-85747 Garching, Germany*

T. Leininger and F. X. Gadea

*Laboratoire de Physique Quantique, L'Institut de Reckercke sur les Systemes Atomiques et Moleculaires Complexes, Université Paul Sabatier, 118 Route de Narbonne, Toulouse Cedex, France*

(Received 19 June 2000; published 9 May 2001)

Low-energy electron collisions with the HBr and DBr molecules are addressed from the experimental and theoretical points of view. Relative differential cross sections for the excitation of vibrational levels of HBr and DBr up to  $v=6$  have been measured as a function of the incident electron energy in the range 0–4 eV. In addition to the shape resonance near 2 eV collision energy, intense and narrow threshold peaks are found for the excitation of the  $v=1$  level of HBr and the  $v=1$  and  $v=2$  levels of DBr. Measurements with high resolution for rotationally cooled molecules have revealed the existence of sharp oscillatory structures in the elastic and  $v=0\rightarrow 1$  cross sections in a narrow range below the dissociative-attachment threshold. The dissociative-attachment cross section has been measured with high resolution of the incident electrons in the range 0.2–1.4 eV. The theoretical analysis is based on an improved nonlocal resonance model, which has been constructed on the basis of existing fixed-nuclei electron-HBr scattering phase shifts and accurate *ab initio* calculations of the bound part of the  $\text{HBr}^-$  potential-energy function. This purely *ab initio*-based model is used to calculate integral electron-scattering and dissociative-attachment cross sections for HBr and DBr. The theoretical cross sections agree very well with the experimental data. The observed threshold peaks and Wigner cusp structures in the vibrational excitation functions are correctly reproduced. The sharp structures in the  $v=0\rightarrow 0$  and  $v=0\rightarrow 1$  cross sections below the dissociative-attachment threshold, consisting of a superposition of boomerang-type oscillations and quasibound levels of the outer well of the  $\text{HBr}^-$  potential-energy function, are quantitatively described by the theory. The high degree of agreement between experiment and theory indicates that the essentials of low-energy electron-HBr collision dynamics are completely understood.

DOI: 10.1103/PhysRevA.63.062710

PACS number(s): 34.80.Ht, 34.50.Ez, 31.15.Ar

**I. INTRODUCTION**

The discovery of pronounced threshold peaks in the vibrational excitation (VE) cross sections of HF, HCl, and HBr by Rohr and Linder [1–3] has initiated intense experimental and theoretical research on low-energy collisions with hydrogen halides. A survey of the experimental developments has been given by Cvejanović [4]. The theoretical developments have been reviewed by Morrison [5], Fabrikant [6], Domcke [7], and Horáček [8].

Recently, not only more definitive determinations of the shape and intensity of the threshold peaks in the VE functions of hydrogen halides have become possible, but also additional unexpected phenomena have been discovered. A detailed study of rovibrational excitation functions of HF and HCl has been performed by Ehrhardt and collaborators, leading to the discovery of vibrational Feshbach resonances in the  $e + \text{HF}$  collision system [9]. Very recently, Allan and co-workers [10] extended the measurements up to the  $v=4$  channel in HF, providing additional data on vibrational Feshbach resonances and establishing the existence of oscillatory structures (so-called boomerang oscillations [11]) in

the  $v=3$  and  $v=4$  excitation functions of HF. Calculations of  $e + \text{HCl}$  VE cross sections with an improved version of the so-called nonlocal resonance model [12], which is based on *ab initio* electron-HCl scattering data as well as accurate *ab initio* calculations of the bound part of the  $\text{HCl}^-$  potential-energy function, have predicted the existence of surprisingly sharp and intense oscillatory structures in the  $v=1$  and  $v=2$  excitation functions of HCl in a narrow energy range below the dissociative attachment (DA) threshold [13]. Indications of this structure have been observed in measurements of Cvejanović and Jureta [4] and Schafer and Allan [14]. In a recent high-resolution measurement of electron scattering in cooled HCl, quantitative agreement of the measured and calculated structures has been established [15]. The observed structures were shown to consist of a superposition of boomerang oscillations, reflecting short-lived wavepacket motion of the  $\text{HCl}^-$  anion, and so-called outer-well resonances, arising from quasibound energy levels in the outer well (centered at an internuclear distance of about 4 a.u.) of the  $\text{HCl}^-$  potential-energy function [13,15].

The electron-HBr collision system has received much less attention than the electron-HCl system. It has been pointed

out by Azria *et al.* [16] that the threshold peaks in higher vibrational channels reported by Rohr [3] are likely to be artifacts, arising from the lack of discrimination of slow electrons and  $\text{Br}^-$  anions. A calculation of VE cross sections within the nonlocal resonance model indeed predicted the existence of threshold peaks only for the  $0 \rightarrow 1$  channel in HBr and the  $0 \rightarrow 1$  and  $0 \rightarrow 2$  channels in DBr [17]. This finding correlates with the fact that only the  $v=0$  and  $v=1$  levels of HBr are located below the DA threshold, while the  $v=0, 1$ , and 2 levels of DBr are below the DA threshold. The calculation also predicted the existence of very sharp structures in the VE cross sections just below the DA threshold [17].

Cross sections for VE of HI, finally, have been measured recently [18]. In agreement with a model calculation of Horáček *et al.* [19], extended Wigner cusp structures are found at the vibrational thresholds, but no threshold peaks. While the shape of the theoretically predicted excitation functions is qualitatively correct, the decrease of the cross sections with increasing inelasticity is significantly too weak, indicating the need of improvement of the theoretical model [18].

In the present paper, we add new experimental and theoretical results on the electron-HBr/DBr collision system to supplement the existing picture of low-energy electron collisions with hydrogen halides. The experimental part of this paper comprises measurements of relative differential cross sections using two complementary instruments. A magnetically collimated spectrometer measures vibrationally inelastic cross sections (at  $0^\circ$  and  $180^\circ$ ) and provides a stable response function near threshold. The high sensitivity of this instrument has permitted measurements up to the  $v=0 \rightarrow 6$  transition in both HBr and DBr. To reveal the existence of fine structure in the elastic and the  $v=0 \rightarrow 1$  cross sections, a spectrometer with hemispherical electrostatic analyzers is used. The response function of this instrument is less stable near threshold, but it has a higher resolution required to reveal narrow structures. The electrostatic instrument has also been used to measure relative dissociative electron attachment cross sections.

In the theoretical part, we report on *ab initio* calculations of potential-energy functions of HBr and  $\text{HBr}^-$ , employing very large basis sets and a sophisticated treatment of electron-correlation effects. Making use of these results as well as published electron-HBr scattering data [20], an improved nonlocal resonance model for electron-HBr collisions is developed. Extensive calculations of VE and DA cross sections are performed for this model on a very fine energy grid, using the previously developed Schwinger-Lanczos approach [17,21–23].

To allow for a detailed comparison between experiment and theory, the theoretical data have been appropriately averaged over the rotational population distribution of the target gas and convoluted with an experimental resolution function. The comparison of the resulting cross sections with experiment reveals a high degree of agreement, even for fine details of the sharp structures in the cross sections. While there is still a need for improvement of the quantitative accuracy of the calculations, especially at higher collision en-

ergies, the present results suggest that all qualitative aspects of the complex resonance and threshold phenomena in low-energy electron-HBr/DBr scattering are well understood.

The theoretical model also yields cross sections for the alternative channel of associative detachment (AD). The results for the AD cross section, in particular energy spectra of the detached electrons, are reported in Ref. [52].

## II. EXPERIMENTAL METHODS

The ‘‘trochoidal’’ electron spectrometer, used already in our earlier study of HCl [14], and more recently of HI [18] and HF [10], has been described in more detail in Refs. [24–26]. It is particularly suitable for the study of threshold features, because the collimating action of the axial magnetic field (about 80 Gauss) results in a stable response function even for slow electrons. Its high sensitivity has permitted recording the cross section up to the  $v=0 \rightarrow 6$  transition.  $\text{Br}^-$  ions from dissociative electron attachment cannot pass trochoidal analyzers and do not reach the detector. The present spectra are consequently not affected by artifact signals due to unwanted detection of anions, which may occur with instruments employing purely electrostatic guidance of electrons, as pointed out by Azria *et al.* [16].

The calibration of energy scales, correction of the raw data for the instrumental response function, and other technical aspects of recording the spectra of hydrogen halides, have been described in the recent publication on HF [10]. The instrument uses a trochoidal monochromator [27] to prepare a quasimonoenergetic electron beam and two trochoidal analyzers in series to select the energy of the scattered electrons. The electrons collide with a quasistatic gas sample in a collision chamber. Both forward and backward-scattered electrons are detected [25,26]. The count rate of the scattered electrons is recorded as a function of the residual electron energy, subsequently corrected for the response function of the energy analyzer, and finally plotted as a function of the incident electron energy. The confidence limits of the correction procedure are taken to be  $\pm 20\%$  in the residual energy range 0.1–3 eV and  $\pm 35\%$  below 0.1 eV. The residual energy scale was calibrated on a sharp resonance feature in the excitation of the  $2^3\text{P}$  state of helium as described previously [10]. It is accurate to within  $\pm 30$  meV. The temperature of the target chamber was about  $60^\circ\text{C}$ . The excitation functions were measured at the peaks of the vibrational bands, emphasizing  $\Delta J=0$  transitions. The resolution (monochromator and analyzer combined) was 60 meV. The instrumental band pass was thus comparable to the rotational bandwidth, causing partial integration over rotational transitions.

The sample pressure plays a critical role in the present measurements. The very large total scattering cross section of polar molecules at low energies causes noticeable attenuation of slow scattered electrons and consequently a noticeable attenuation or disappearance of the threshold peak already at surprisingly low pressures. Spectra were therefore recorded at successively lower pressures until a pressure was found below which the shape of the excitation functions no longer changed. The pressure in the main chamber of the

instrument was then below the sensitivity of the cold cathode gauge, that is less than  $10^{-7}$  mbar, indicating a pressure of less than  $10^{-4}$  mbar in the target chamber.

The spectrometer with hemispherical analyzers also has already been described [28,29]. It has been used to measure the elastic cross section, which is not accessible to the magnetically collimated instrument, and to better visualize the oscillatory structure in some of the cross sections, where higher resolution was necessary. A simple Wien filter, permitting the separation of scattered electrons and fragment anions, is incorporated in front of the detector. The filter has been used to positively eliminate ion signal from the spectra of scattered electrons, and to record dissociative electron attachment spectra.

HBr or DBr without carrier gas was expanded from a 30- $\mu$ m orifice, with backing pressures of about 0.2–0.5 bars. Narrowing of the HBr elastic energy-loss peak with increasing backing pressure indicated significant cooling, although the exact temperature was not known. The analyzer response function was determined on the elastic scattering and on the ionization continuum near threshold in helium. The resolution of the instrument in the energy-loss mode (determined on the elastic peak of helium) was slightly below 20 meV full width at half maximum (FWHM), corresponding to an energy spread of about 14 meV in the incident beam. The energy of the incident beam was calibrated on the 19.366 eV  $^2$ S resonance in helium and is accurate to within  $\pm 20$  meV. The excitation functions have been recorded at the maxima of the energy-loss peaks and emphasize consequently the  $\Delta J=0$  transitions. The dissociative attachment spectra have been recorded with a backing pressure about 5 times smaller than the elastic and VE spectra to reduce the effect of secondary collisions of the  $\text{Br}^-$  ions with the sample gas, and to reduce the expansion cooling, permitting observation of fragment anion signal from thermally rotationally and vibrationally excited molecules.

The response function of the hemispherical instrument is not very stable at low energies. The collection efficiency varies dramatically as a consequence of only small variations of the potentials in the target region. The shape of the curves recorded with this instrument from threshold to about 0.6 eV above is thus only qualitative. The results from the magnetically collimated instrument are more reliable as far as threshold peaks are concerned.

### III. THEORETICAL METHODS

#### A. *Ab initio* calculation of potential-energy functions

The *ab initio* calculation of heavy element compounds takes benefit from valence-only approaches, where the computational effort can be concentrated on molecular interactions of mainly valence character. Large basis sets have been used here for both atoms:  $\text{Br}(22s,17p,11d,4f,3g)$  and  $\text{H}(9s,5p,4d,3f,2g)$ , together with a pseudopotential for Br. Although weak core-valence effects are expected for bromine (seven valence electrons), this correlation energy has to be taken into account adequately in order to reach a good accuracy. For the neutral molecule in its ground state very accurate results were obtained by Dolg [30] with an energy-

adjusted quasirelativistic pseudopotential and an estimation of the core-valence correlation energy. We have here followed a similar approach and have adopted the uncontracted basis sets, the pseudopotential and the core polarization potential [31] of Ref. [30]. Except for the core, where they are taken into account in an average way, relativistic effects are not considered in the present *ab initio* calculation. Spin-orbit coupling plays an important role in the production of  $\text{H}^-$  by dissociative attachment, through nonadiabatic transitions involving excited states of the anion that dissociate in  $\text{H}^- + \text{Br}$  [32]. Although the fine structure of Br is important there, we are interested here in the ground state of the  $\text{HBr}^-$  anion, which involves mainly a closed shell  $\text{Br}^-$  atom without fine structure.

The *ab initio* calculations were performed with the MOLPRO [33] package. In all cases, molecular orbitals were optimized according to a minimal complete active space calculation. It involves eight configurations for the neutral molecule and three for the anion. Preliminary calculations at the coupled-cluster level of theory for HBr have shown incorrect behavior of the energy at large distances as the molecule dissociates in two open shell atoms. A multireference expansion of the wave function is thus indispensable. To get reliable results over a wide range of internuclear distances, from short internuclear distances to the asymptotic limit, we have adopted the average quadratic coupled cluster (AQCC) method [34]. It is only quasisize consistent, but allows for a multireference configuration interaction (CI) expansion. In addition, excited states also can be investigated. Moreover, a previous study [35] devoted to the  $\text{Cl}_2$  molecule has shown the suitability of the AQCC method for the *ab initio* investigation of electron attachment to molecules with heavy halogen atoms, being preferable to perturbative approaches such as complete active space second-order perturbation theory (CASPT2) or complete active space third-order perturbation theory (CASPT3).

As a first check of the quality of the *ab initio* calculation of the potential-energy function, the separated atom limit should be considered. This limit represents a particularly challenging problem here, since the electron-attachment process involves different species, a neutral HBr, and an anionic  $\text{HBr}^-$ , which are asymptotically separated by the electron affinity (EA) of Br. For the EA we get 3.373 eV for Br (exp: 3.364 eV [36]) and 0.7466 eV for H (exp: 0.7542 eV [36]). We have thus obtained a very good accuracy for the asymptotic limits.

The spectroscopic data for the ground state of HBr are reported in Table I in comparison with previous calculations and experiment. Our results are very similar to the calculation of Dolg [30], although not identical, and in much better agreement with experiment than the spin-orbit configuration interaction (SOC) calculation of Chapman *et al.* [37]. The latter calculation has used a different pseudopotential, smaller basis sets and much smaller CI expansions, resulting in a well which is less deep, at larger distance, and too wide. Average coupled pair functional (ACPF) and AQCC methods only differ by the extrapolation of the coupled-pair correlation energy and are expected to yield a similar accuracy. For the binding energy we have a small discrepancy with the

TABLE I. Spectroscopic constants for the ground state of HBr. The units are  $\text{\AA}$  for  $R_e$ , eV for  $D_e$ , and  $\text{cm}^{-1}$  for  $\omega_e$ .

	$D_e$	$R_e$	$\omega_e$
SOCI [37]	3.81	1.42	2561
CCSD(T) [30]	4.09	1.410	2670
CCSD(T)+SO [30]	3.95	1.410	2666
ACPF [30]	4.07	1.410	2668
ACPF+SO [30]	3.93	1.410	2663
AQCC <sup>a</sup>	4.05	1.410	2662
AQCC+SO <sup>b</sup>	$\approx 3.91$	$\approx 1.410$	$\approx 2657$
Exp [39]	3.92	1.414	2649

<sup>a</sup> $\omega_e$  results from a three-level fit ( $\omega_e x_e = 52 \text{ cm}^{-1}$ ).

<sup>b</sup>SO effect estimated, see text.

result of Dolg [30]. However, it was computed there with respect to the separated atoms while we have used, as reference, large-distance molecular calculations, large enough (50–100 a.u.) to be in the asymptotic limit. Since neither AQCC nor ACPF are strictly size consistent, a small discrepancy remains between the molecular and separated-atoms calculations. In our case (AQCC) it amounts to 0.017 eV and mainly accounts for the small difference between the ACPF result (4.07 eV [30]) and the present AQCC result (4.05 eV).

As is well known [38], spin-orbit (SO) interactions affect much more the asymptotic region, where quasidegeneracy arises, than the molecular energies near  $R_e$  where the covalent interactions produce large energy separations. Therefore, for the spectroscopic constants, the main SO effect is often a decrease in  $D_e$  as a consequence of the atomic fine-structure splitting, whereas  $R_e$  and  $\omega_e$  remain almost unchanged. Inspection of the coupled-cluster singles and doubles including perturbative triples [CCSD(T)] and ACPF results of Dolg [30] with and without SO, confirms this analysis. For both methods,  $D_e$  decreases by 0.14 eV due to SO coupling whereas there is not any change for  $R_e$  and only a minor one for  $\omega_e$ . We can safely estimate the SO correction to lead here to the same decrease for  $D_e$ , giving 3.91 eV, in excellent agreement with the experimental value 3.92 eV [39]. The good accuracy obtained for the neutral molecule, as documented in Table I, strongly supports the reliability of the present *ab initio* approach for the less known anion.

The adiabatic Born-Oppenheimer potential-energy curves for HBr and the electronically bound part of  $\text{HBr}^-$  are illustrated in Fig. 1. The calculated ground-state energy of the anion exhibits a minimum and a barrier near the crossing with the potential energy of the neutral molecule. A similar shape has been obtained by Chapman *et al.* [37]. The electronically bound part of the first excited-state potential-energy function of  $\text{HBr}^-$  is also included in Fig. 1. This potential function is repulsive, dissociating into  $\text{H}^- + \text{Br}$ . It should be stressed that the Ritz variational principle, on which the present *ab initio* calculations are based, applies only for bound electronic states, but not for electronic states in the continuum (resonances). For continuum wave functions, the expansion in terms of square-integrable basis functions does not converge. For the internuclear distances below crossing point of HBr and  $\text{HBr}^-$  potentials we therefore re-

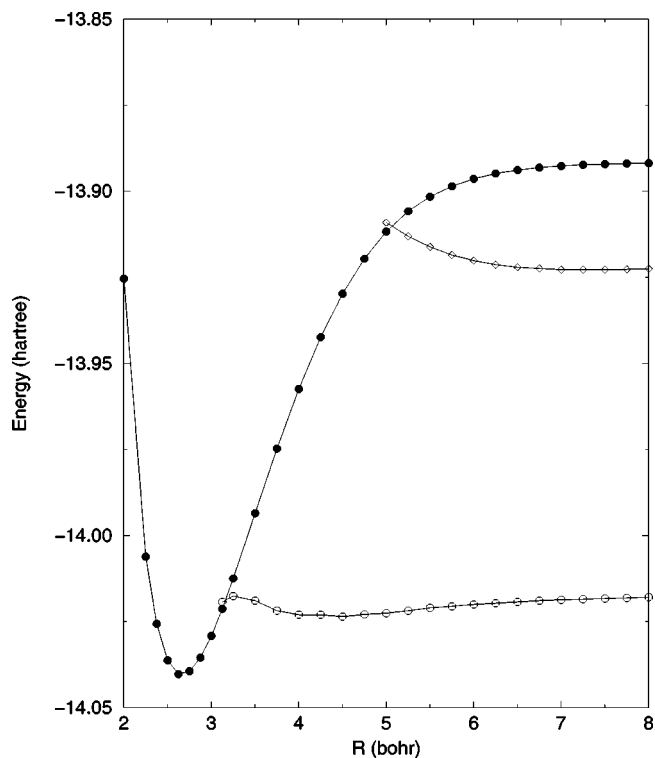


FIG. 1. *Ab initio* potential-energy curves for HBr ( $^1\Sigma$  ground state) and the two lowest  $^2\Sigma$  states of  $\text{HBr}^-$ , computed with the AQCC method. Filled symbols label the neutral curve, while unfilled ones label the anionic curves.

lied on *ab initio*  $e^- + \text{HBr}$  scattering data as a basis for the calculation of the dynamics (see Sec. III). The nonlocal resonance model to be discussed below, which is based on scattering theory, predicts the following behavior of the  $\text{HBr}^-$  potential-energy function near the crossing with the HBr potential: the  $\text{HBr}^-$  energy joins the HBr energy from below and follows it down to a certain critical distance, before it switches into the continuum, representing the  $^2\Sigma^+$  shape resonance (cf. Sec. III C). As will become clear below, the wide and shallow outer well and the barrier separating the inner part from the outer well are important features of the  $\text{HBr}^-$  ground-state potential-energy function. A very similar shape of the potential-energy function has previously been found for  $\text{HCl}^-$  [40,41]. It is to be expected that the height of the barrier is overestimated by the present calculation owing to basis-set limitations.

The calculated dipole-moment function of HBr is displayed in Fig. 2. The shape of this function is in agreement with previous calculations [42]. The dipole moment at the equilibrium geometry of HBr is 0.810 D. This value agrees well with previous theoretical estimates [0.819D self-consistent electron pairs (SCEP)/coupled electron pair approximation (CEPA) [42]], 0.820D (SOCI [37]), 0.797D (ACPF [30]) and the experimental value (0.820D [39]). The dipole-moment function enters into the nonlocal resonance model via the determination of the threshold exponent [7,22].

Spectroscopic data for the outer well of the  $\text{HBr}^-$  ground state are collected in Table II. Although the present calcula-

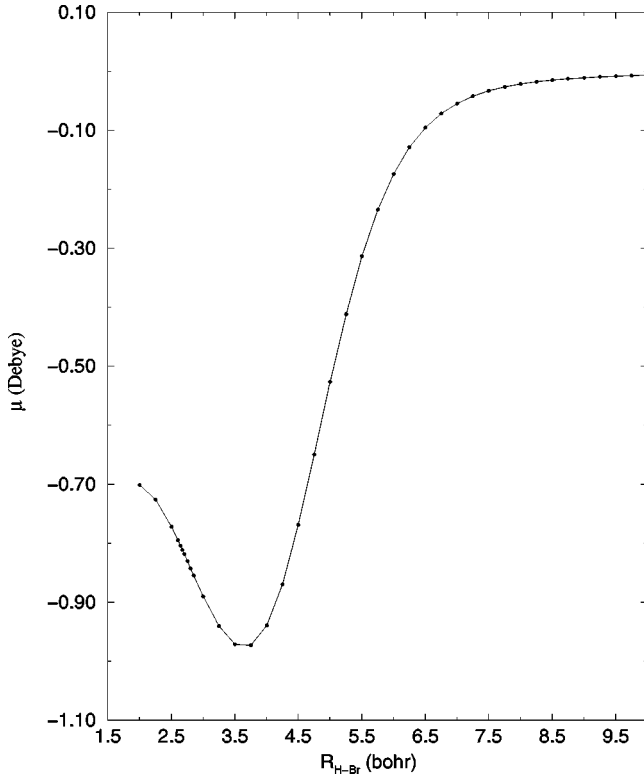


FIG. 2. Dipole-moment function of the  $^1\Sigma$  ground state of HBr.

tion involves larger basis sets and about 800 000 uncontracted configurations, a factor of about 40 larger than the previous calculation [37], the spectroscopic constants for the outer well are not very different, indicating that this part of the energy function is robust. We got a slightly deeper well at a somewhat shorter distance than in Ref. [37]. The outer well is wide enough to support several vibrational levels. As mentioned above, SO effects are not expected to play an important role for the ground-state potential-energy function.

### B. Nonlocal resonance formalism and calculation of cross sections

A detailed description of the nonlocal resonance formalism has been given elsewhere [7,23]. Here we give only a brief overview in order to introduce the model.

The basic assumption of the nonlocal resonance formalism is that a temporary molecular negative-ion state is formed in the collision. This resonance state is approximately described by a square-integrable function  $|\varphi_d\rangle$ , which is assumed to interact with a continuum of states  $|\varphi_\epsilon\rangle$  or

TABLE II. Spectroscopic constants for outer well and barrier in the ground state of  $\text{HBr}^-$ . The units are  $\text{\AA}$  for  $R_e$ , eV for  $D_e$ , and  $\text{cm}^{-1}$  for the zero-point energy.

	$D_e$	$R_e$	ZPE
Outer well	0.156	2.257	200
Outer well [37]	0.14	2.38	201
Barrier	0.074	1.763	

thogonal to  $|\varphi_d\rangle$ . The state  $|\varphi_\epsilon\rangle$  describes an electron with energy  $\epsilon$  scattered by the neutral molecule in its ground electronic state. The coupling between the discrete state and the continuum is determined by the coupling amplitude  $V_{d\epsilon}(R) = \langle \varphi_d | H_{\text{el}} | \varphi_\epsilon \rangle$ , which depends on the separation  $R$  of the nuclei. With  $H_{\text{el}}$  we denote the electronic part of the Hamiltonian,  $H = T_N + H_{\text{el}}$ , where  $T_N = -\Delta_R/2\mu$  is the kinetic energy of the nuclei.

It is possible to show that a proper choice of  $|\varphi_d\rangle$  ensures diabaticity of the states  $|\varphi_\epsilon\rangle$  and that these states form a convenient basis to expand the Hamiltonian [7]

$$\begin{aligned}
 H = & T_N + |\varphi_d\rangle V_d(R) \langle \varphi_d| + \int d\epsilon d\Omega |\varphi_\epsilon\rangle [V_0(R) + \epsilon] \\
 & \times \langle \varphi_\epsilon| + \int d\epsilon d\Omega |\varphi_d\rangle V_{d\epsilon}(R) \langle \varphi_\epsilon| \\
 & + \int d\epsilon d\Omega |\varphi_\epsilon\rangle V_{d\epsilon}^* \langle \varphi_d|,
 \end{aligned} \quad (1)$$

where  $V_d(R) = \langle \varphi_d | H_{\text{el}} | \varphi_d \rangle$  is the discrete-state potential and  $V_0$  is the potential energy of the neutral molecule in its ground state. With  $\int d\Omega$  we denote the integration over the direction of the asymptotic wave vector of the electron.

To solve the Lippmann-Schwinger equation describing electron-HBr scattering, the wave function  $\Psi(R, r)$  is expanded into the basis set  $|\varphi_d\rangle = \varphi_d(R, r)$ ,  $|\varphi_\epsilon\rangle = \varphi_\epsilon(R, r)$  ( $r$  denotes all electronic degrees of freedom) as

$$\Psi(R, r) = \psi_d(R) \varphi_d(R, r) + \int d\epsilon \psi_\epsilon(R) \varphi_\epsilon(R, r). \quad (2)$$

It is possible to show that the coefficient  $\psi_\epsilon$  can be eliminated from the equations of motion [7] and after partial-wave decomposition [23,43] of  $\psi_d(R)$  the equation for its partial wave component  $\psi_J(R)$  is found to be ( $J$  is the quantum number of total angular momentum)

$$|\psi_J\rangle = |\phi_J\rangle + G_J(E) [V_d + F_J(E)] |\psi_J\rangle, \quad (3)$$

where

$$\langle R | F_J(E) | R' \rangle = \int d\epsilon d\Omega V_{d\epsilon}(R) g_J(E - \epsilon, R, R') V_{d\epsilon}^*(R') \quad (4)$$

and

$$g_J(E) = \left( E + \frac{1}{2\mu} \frac{d^2}{dR^2} - V_0(R) - \frac{J(J+1)}{2\mu R^2} + i\epsilon \right)^{-1}. \quad (5)$$

Adopting boundary conditions appropriate for electron-molecule scattering, the function  $|\phi_J\rangle$  is given by

$$|\phi_J\rangle = G_J(E) V_{d\epsilon_i} |\chi_J^{\nu_i}\rangle, \quad (6)$$

where  $|\chi_J^{\nu_i}\rangle$  denotes the initial rovibrational state of the molecule ( $\nu_i$  is the vibrational quantum number),  $\epsilon_i$  is the initial

energy of the electron, and  $G_J(E)$  is the partial-wave component of the free Green's function. The cross section for vibrational excitation reads

$$\sigma_{\text{VE}} = \frac{2\pi^3}{\epsilon_i} |\langle \chi_J^{\nu_f} | V_{d\epsilon}^* | \psi_J^{\nu_i} \rangle|^2, \quad (7)$$

with the final energy of the scattered electron given by energy conservation,  $\epsilon_i + E_J^{\nu_i} = \epsilon_f + E_J^{\nu_f}$ . The quantity  $E_J^{\nu}$  represents the energy of the neutral molecule in the state  $|\chi_J^{\nu}\rangle$ .

We should add the following comment on the coupling element. In general, the coupling element  $V_{d\epsilon}(R)$  depends on the angle  $\theta$  between the molecular axis and the direction of the incoming electron. The coupling element can be expressed in the form of a partial-wave expansion

$$V_{d\epsilon}(R) = \sum_l \sqrt{\frac{2l+1}{4\pi}} P_l(\cos \theta) V_{d\epsilon l}(R). \quad (8)$$

In the present theoretical treatment we neglect all terms with  $l > 0$ . The partial-wave component of the wave function with a certain  $J$  is thus coupled to states of the neutral molecule with the same  $J$  only [see Eq. (4)], i.e., our model cannot describe rotational excitation by electron impact. As a consequence of this assumption, we have to solve Eq. (3) only for a single value of  $J$ , which is given by the initial angular momentum of the molecule.

The VE cross sections are obtained from Eq. (7), where the wave function  $|\psi_J\rangle$  is the unique solution of the Lippmann-Schwinger equation (3). To solve this equation we employ the Schwinger-Lanczos method, which proved to be very efficient for the calculation of VE and DA cross sections for  $\text{H}_2$ ,  $\text{HCl}$ ,  $\text{HBr}$ , and  $\text{HI}$  molecules [23,13,17,19]. For a detailed description of the Schwinger-Lanczos method, see Ref. [21]. For the treatment of the nonseparability of the coupling matrix element  $V_{d\epsilon}(R)$  due to the variable threshold exponent and cutoff parameter (see below) we use the Batemann technique described in Ref. [22].

### C. Construction of the nonlocal resonance model

A nonlocal resonance model for the  $e+\text{HBr}$  system has previously been developed by Horáček and Domcke [17]. This model was obtained by fitting *ab initio* fixed-nuclei electron-HBr scattering data of Fandreyer *et al.* [20]. Here we describe the construction of an improved model. For short internuclear distances the same *ab initio* scattering data are used, while the long-range part of the  $\text{HBr}^-$  potential-energy function is modeled more carefully on the basis of the new  $\text{HBr}^-$  *ab initio* data of Sec. III A. Moreover, the dependence of the threshold exponent on the internuclear distance is taken into account.

The nonlocal resonance model is described by three functions: the discrete-state potential  $V_d(R)$ , the potential of the neutral molecule  $V_0(R)$ , and the discrete-state-continuum coupling  $V_{d\epsilon}(R)$ . We used, for the construction of the new model, the following data:

(i) *Ab initio* calculations of the fixed-nuclei eigenphase sum for  $^2\Sigma$  symmetry performed by Fandreyer *et al.* [20].

(ii) *Ab initio* calculations of the  $\text{HBr}^-$  negative ion state at intermediate and large values of the internuclear distance, see Sec. III A.

(iii) *Ab initio* calculation of the dipole moment of  $\text{HBr}$ , also see Sec. III A. The dipole moment determines the dependence of the threshold exponent on the internuclear distance.

(iv) The polarizability of the hydrogen atom that determines the long-range part of the  $\text{Br}^-$ -H interaction.

The potential  $V_0(R)$  of the ground electronic state of  $\text{HBr}$  is as in the previous model [17] described by the Morse function

$$V_0(R) = D_0 [e^{-2\alpha_0(R-R_0)} - 2e^{-\alpha_0(R-R_0)}], \quad (9)$$

with  $R_0 = 2.67$  a.u.,  $\alpha_0 = 0.96$  a.u., and  $D_0 = 3.92$  eV. The parameters were fitted to the spectroscopic data given in Table I, which are essentially identical with the experimental data [39].

$V_d(R)$  and  $V_{d\epsilon}$  can be inferred by fitting a Breit-Wigner formula with energy-dependent width and level shift [12] to the *ab initio* eigenphase sum

$$\delta(\epsilon, R) = \delta_{\text{bg}}(\epsilon, R) - \tan^{-1} \left( \frac{\frac{1}{2}\Gamma(\epsilon, R)}{\epsilon - V_d(R) + V_0(R) - \Delta(\epsilon, R)} \right), \quad (10)$$

where

$$\Gamma(\epsilon, R) = 2\pi |V_{d\epsilon}(R)|^2 \quad (11)$$

and

$$\Delta(\epsilon, R) = \frac{1}{2\pi} P \int \frac{\Gamma(\epsilon', R)}{\epsilon - \epsilon'} d\epsilon'. \quad (12)$$

The background eigenphase sum  $\delta_{\text{bg}}(\epsilon, R)$  is assumed to be a smooth function of  $\epsilon$  and  $R$ .

It is assumed that  $\Gamma(\epsilon, R)$  is of the form

$$\Gamma(\epsilon, R) = A(R) \epsilon^{\alpha(R)} e^{-\beta(R)\epsilon}. \quad (13)$$

Here,  $\alpha(R)$  represents the threshold exponent, which depends on the dipole moment of the neutral molecule [12,22]. The dipole moment function of  $\text{HBr}$  has been discussed in Sec. III A. Since the present calculation of the dipole moment essentially confirms the data obtained earlier by Ogilvie *et al.* [44], we use their Padé approximation to the dipole moment

$$M(R) = M_0(1+x)^3 \left( 1 + \sum e_i x^i \right)^{-1}, \quad (14)$$

where  $x = (R - R_0)/R_0$  and  $M_0 = 0.81788$ ,  $e_1 = 2.199$ ,  $e_2 = 0.808$ ,  $e_3 = 1.483$ ,  $e_4 = 3.868$ ,  $e_5 = -2.612$ ,  $e_6 = 13.209$ , and  $e_7 = 0.255$ . The threshold exponent can then be approximately represented by a simple formula [22]

$$\alpha(R) = \frac{1}{2} + a_1 M^2 + a_2 M^4 + a_3 M^6 + a_4 M^8, \quad (15)$$

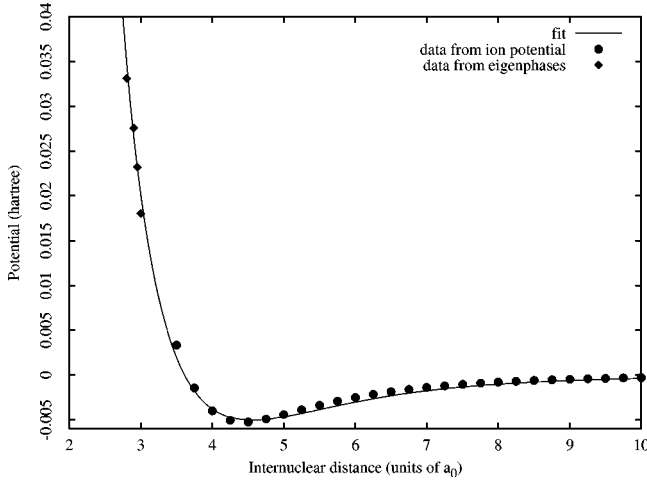


FIG. 3. Construction of the discrete state potential  $V_d(R)$  by interpolation of *ab initio* data from the fixed-nuclei  ${}^2\Sigma$  eigenphase sum (diamonds) and the  ${}^2\Sigma$  bound state of  $\text{HBr}^-$  (circles).

with  $a_1 = -0.101157$ ,  $a_2 = -1.4833 \times 10^{-2}$ ,  $a_3 = 7.486 \times 10^{-3}$ , and  $a_4 = 3.735 \times 10^{-3}$ .

To find suitable forms of the functions  $A(R)$  and  $\beta(R)$  in Eq. (13) we first fitted the eigenphase sum of Fandreyer *et al.* for each  $R$  separately, using Eq. (10). For the background eigenphase we assumed the form

$$\delta_{\text{bg}}(\epsilon, R) = \frac{\pi}{2} \left( \frac{1}{2} - \alpha(R) \right) + a(R)\epsilon^{\alpha(R)} + b(R)\epsilon \quad (16)$$

in accordance with Ref. [17]. The best least-squares fit gives five quantities,  $V_d$ ,  $A$ ,  $\beta$ ,  $a$ , and  $b$ , for each of the 13 values of  $R$  between 2.0 and 3.1 a.u. for which the eigenphases were published. We found that a very good fit of the eigenphases is obtained assuming a constant  $b(R)$  and linear functions  $a(R)$ ,  $\beta(R)$ , and  $g(R) \equiv \sqrt{A(R)\beta(R)}^{-\alpha(R)/2}$ . We assume that the same linear form of  $\beta(R)$  and  $g(R)$  can also be used at larger internuclear distances,  $R > 3.1$  [ $g(R)$  crosses the  $x$  axis at  $R = 4.73$  a.u. and we put  $g(R) = 0$  for larger  $R$ ].

The negative-ion potential function  $V_i(R)$ , representing a shape resonance for  $V_i(R) > V_0(R)$  and a bound state for  $V_i(R) < V_0(R)$ , is related to the functions  $V_d(R)$  and  $\Delta(\epsilon, R)$  via [7]

$$V_i(R) = V_d(R) + \Delta(V_i(R) - V_0(R), R). \quad (17)$$

Using the above extrapolations of  $a(R)$ ,  $b(R)$ ,  $\beta(R)$ , and  $g(R)$ , we can evaluate  $V_d(R)$  for  $R > 3.1$  a.u. from Eq. (17) using the *ab initio* data of Sec. III A for  $V_i(R)$ .

The values of  $V_d(R)$  found in this way are shown as circles in Fig. 3. The same figure also contains the values of the discrete state potential  $V_d(R)$  obtained from fitting the *ab initio* eigenphase sum by the Breit-Wigner formula (10) separately for each  $R$  for  $R < 3$  a.u. (diamonds). At large distances, the function  $V_d(R)$  has to approach the polarization potential  $-2.25R^{-4}$  (in a.u.). We suggest the following ansatz for  $V_d(R)$ , which is consistent with all these facts

$$V_d(R) = Ve^{-vR} - 2.25[(R - v_1)^2 + v_2]^{-2}. \quad (18)$$

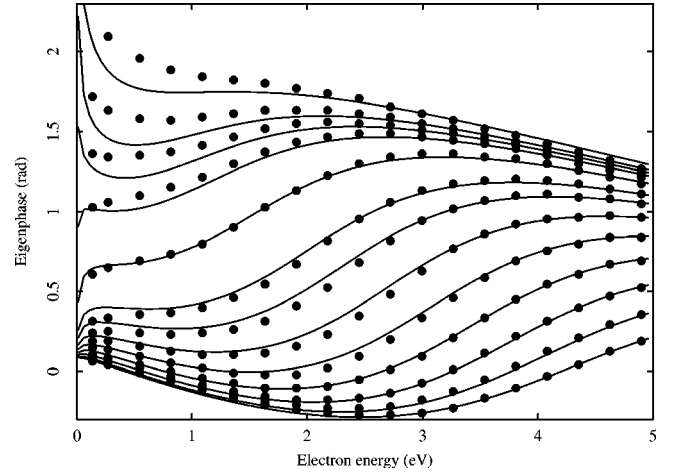


FIG. 4. Fit of the eigenphase sum for fixed- $R$  electron-HBr scattering. The dots are data of Fandreyer *et al.* [20] and solid lines show the fit within the nonlocal resonance model. The corresponding internuclear distances are  $R = 2.0, 2.1, 2.2, 2.3, 2.4, 2.5, 2.6, 2.6729, 2.8, 2.9, 2.95, 3.0,$  and  $3.1$  (from bottom to top).

The best least-square fit was found for  $V = 9.934$ ,  $v = 1.535$ ,  $v_1 = 1.437$ , and  $v_2 = 2.884$ . It is shown in Fig. 3 as the full line seen to provide a satisfactory interpolation of the *ab initio* scattering and bound-state data. To obtain the final form of the width, we used  $V_d(R)$  of Eq. (18) and assumed

$$\Gamma(\epsilon, R) = g(R)^2 [\beta(R)\epsilon]^{\alpha(R)} e^{-\beta(R)\epsilon} \quad (19)$$

for the width and the form (16) for the background with  $g(R)$ ,  $\beta(R)$ , and  $a(R)$  being linear functions and  $b$  being constant. The best least-squares fit to the eigenphase sum of Fandreyer *et al.* [20] was obtained for

$$g(R) = \begin{cases} 0.8688 - 0.1835R & \text{for } R < 4.7345 \\ 0 & \text{for } R > 4.7345, \end{cases} \quad (20)$$

$$\beta(R) = 4.865R - 4.788, \quad (21)$$

$$a(R) = 0.4370R - 4.483, \quad (22)$$

$$b = -2.0281. \quad (23)$$

The resulting nonlocal resonance model for HBr is thus given by the functions  $V_0(R)$  of Eq. (9),  $V_d(R)$  of Eq. (18), and

$$V_d\epsilon(R) = \sqrt{\Gamma(\epsilon, R)/2\pi}, \quad (24)$$

where  $\Gamma(\epsilon, R)$  is given by Eqs. (19)–(23). The eigenphase sum of the final model is compared with the data of Fandreyer *et al.* in Fig. 4.

Figure 5 shows the comparison of the negative-ion potential  $V_i(R)$  derived from the nonlocal resonance model with the *ab initio* data of Sec. III A. The slight disagreement for  $R < 4$  a.u. and the deteriorating fit of the eigenphase sum for  $R$  close to 3 a.u. reflect the incompatibility of the  $\text{HBr}^-$  bound-state calculation with the calculation of eigenphase sum near the crossing point of the potential curves  $V_0(R)$

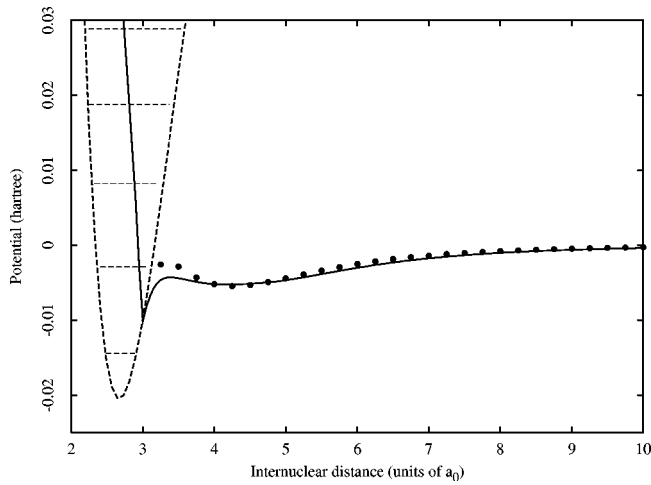


FIG. 5. Potential-energy function of the  $\text{HBr}^-$  ion ground state. *Ab initio* data (this paper) are shown as dots. The full line gives the potential-energy function  $V_i(R)$  of  $\text{HBr}^-$  of the nonlocal resonance model. Potential of the neutral molecule  $\text{HBr}$  is shown with dashes.

and  $V_i(R)$ . For  $R < 3$  a.u. the potential  $V_i(R)$  enters the continuum. The  $V_i(R)$  as defined in Eq. (17) corresponds to the pole of the  $K$  matrix and is thus real. The behavior of the complex poles of the  $S$  matrix in the nonlocal resonance model was analyzed in detail in Ref. [7]. The complex  $S$  matrix poles obtained with the present model (not shown in Fig. 5 for clarity) are in qualitative agreement with the results of Fandreyer and Burke [45] obtained with the *ab initio*  $R$ -matrix method.

## IV. RESULTS

### A. Experimental results

The VE cross sections recorded with the magnetically collimated spectrometer for  $\text{HBr}$  and  $\text{DBr}$  are shown in Figs. 6

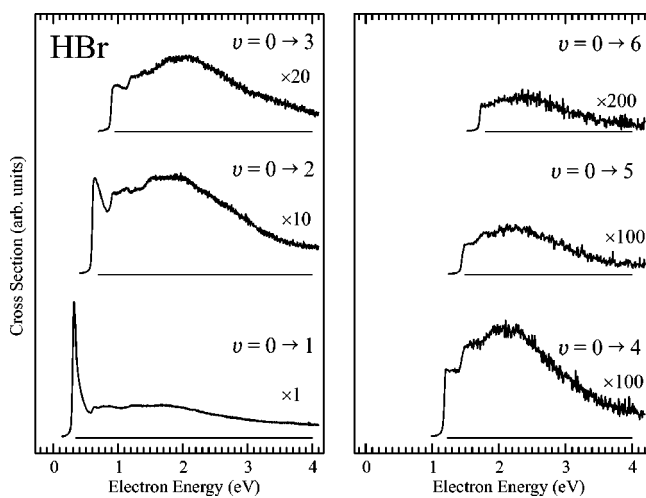


FIG. 6. Cross sections for vibrational excitation in  $\text{HBr}$ , recorded with the magnetically collimated spectrometer. All cross sections are shown on the same (relative) scale, but the curves for the higher vibrational levels are shown vertically expanded as indicated by the multiplication factors.

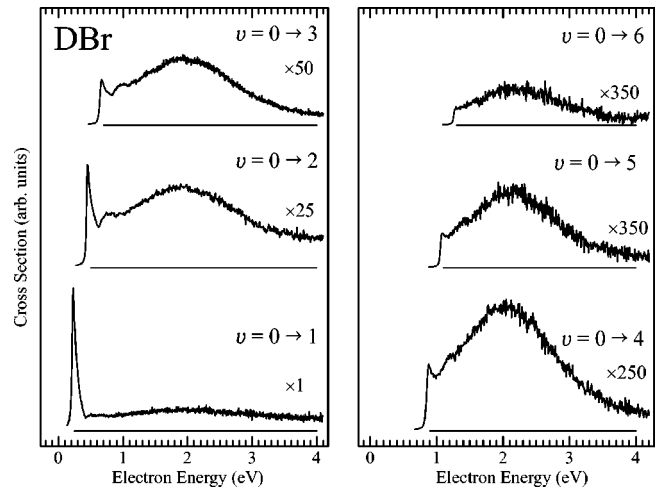


FIG. 7. Cross sections for vibrational excitation in  $\text{DBr}$ , recorded with the magnetically collimated spectrometer and shown in the same format as the  $\text{HBr}$  cross sections in Fig. 6.

and 7. The cross sections for the excitation of low final channels have a narrow peak at threshold, just as in the case of  $\text{HCl}$ , but the highest channel at which a distinct threshold peak is observed is generally less in  $\text{HBr}$  than in  $\text{HCl}$ . A significant threshold peak is observed only in the  $v=0 \rightarrow 1$  channel in  $\text{HBr}$ , while threshold peaks are observed in the  $v=0 \rightarrow 1$  and  $v=0 \rightarrow 2$  channels in  $\text{DBr}$ . At higher energies the cross section has a broad hump around 2 eV.

One of the striking features of VE in  $\text{HCl}$  was the oscillatory structure discovered by Cvejanović in the  $v=0 \rightarrow 1$  and  $v=0 \rightarrow 2$  cross sections, [4,46] and recently reproduced by the nonlocal resonance model [15]. Similar narrow structures have been predicted by the calculation of Ref. [17] for  $\text{HBr}$ . We therefore searched for narrow structures in  $\text{HBr}$  and  $\text{DBr}$  using the spectrometer with electrostatic analyzers. We found structures similar to those of  $\text{HCl}$  in the vibrationally elastic cross sections both in  $\text{HBr}$  (Fig. 8, lower curve) and, less pronounced, in  $\text{DBr}$  (Fig. 9, lower curves).

Only a hint of oscillatory structures is visible (in the form of a shoulder) in the experimental  $v=0 \rightarrow 1$  cross section, shown in the lower part of Fig. 10. The poor visibility is not surprising, however, since the DA limit (0.398 eV) lies only 77 meV above the  $v=1$  vibrational threshold. The structures are thus too dense to be observed clearly. In addition, the collection efficiency of the hemispherical analyzer instrument drops fast at scattered electron energies below 50 meV, distorting the spectrum very close to threshold. Upward and downward steps (Wigner cusps) are seen in the spectrum at the  $v=2$  and  $v=3$  thresholds in Fig. 10. The  $v=1$  vibrational threshold (0.228 eV) is well below the DA threshold (0.440 eV) in  $\text{DBr}$ , permitting a clear observation of oscillatory structure in the  $v=0 \rightarrow 1$  cross section (lower part of Fig. 11).

Figures 12 and 13 show dissociative attachment spectra recorded with the spectrometer with hemispherical analyzers. The Wien filter was set to pass ions and reject scattered electrons. Its resolution is not sufficient to resolve individual ion masses, but only the  $\text{Br}^-$  is formed at the low energies of the present paper. The hemispherical energy analyzer was set



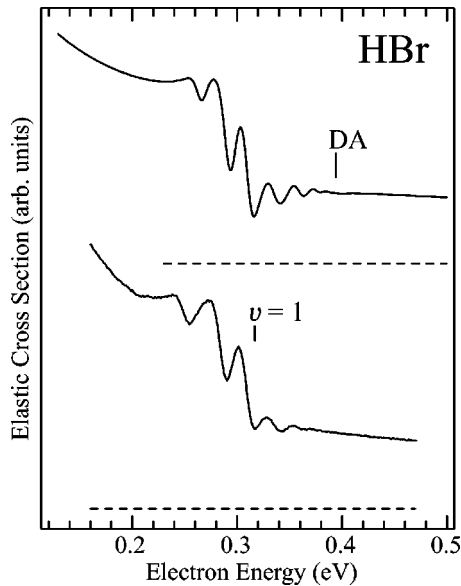


FIG. 8. Vibrationally elastic cross section of HBr. Bottom trace shows the cross section recorded at  $90^\circ$  using the hemispherical analyzer spectrometer. Top trace shows the results of the nonlocal resonance theory, including the broadening caused by thermal rotational excitation of the target at 100 K and convoluted with a Gaussian (5 meV FWHM) to simulate, in part, the finite experimental resolution. The dissociative attachment threshold and the threshold for vibrational excitation are marked.

at the lowest attainable energy, that is, thermal  $\text{Br}^-$  were collected across the entire spectrum. The spectra are thus not affected by variations of the analyzer transmission function with energy, in contrast to the VE cross sections. The re-

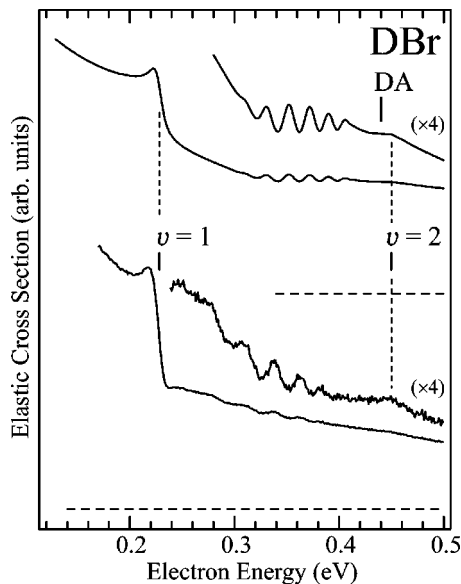


FIG. 9. Experimental (lower part) and theoretical (upper part) vibrationally elastic cross section of DBr. Parts of the curves are shown vertically expanded and offset (the slope of the expanded part of the experimental spectrum is also slightly reduced) to improve the visibility of the structure. (See also explanations in the caption of Fig. 8.)

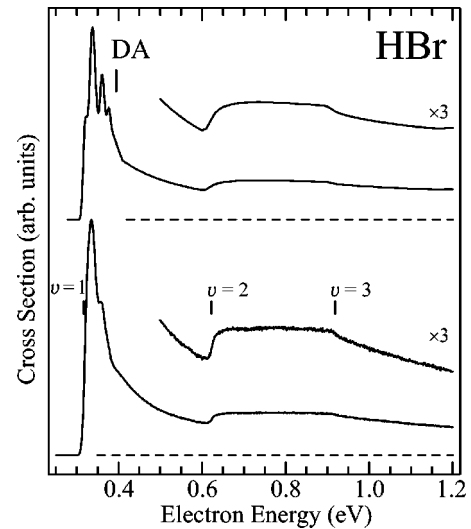


FIG. 10. Experimental (lower part) and theoretical (upper part) cross sections for the  $v=0 \rightarrow 1$  transition in HBr. (See also explanations in the caption of Fig. 8.)

sponse function of the instrument may vary to some degree across the spectrum because the incident electron beam becomes more diffuse at very low energies, but we have not corrected the DA spectra for this variation.

### B. Theoretical results

The theoretical results for the integral vibrational excitation cross section of HBr from  $v=0$  to  $v=1-6$  states are shown in Fig. 14. The cross sections obtained with the previous model of Horáček and Domcke [17] are also included (dashed lines). With the exception of the details near the threshold for  $0 \rightarrow 1$  excitation (to be discussed below), the predictions of the two models are similar. There is a pronounced threshold peak in  $0 \rightarrow 1$  cross section and a sharp

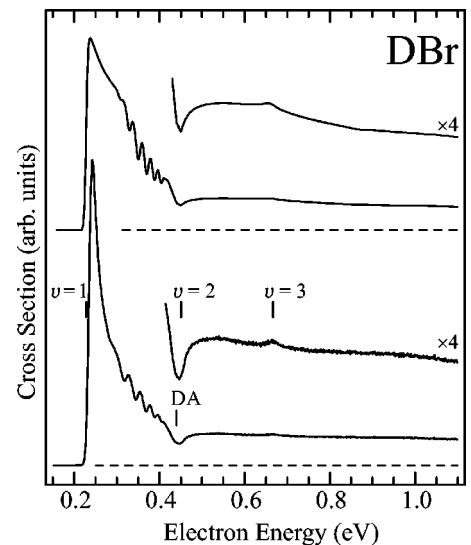


FIG. 11. Experimental (lower part) and theoretical (upper part) cross sections for the  $v=0 \rightarrow 1$  transition in DBr. (See also explanations in the caption of Fig. 8.)

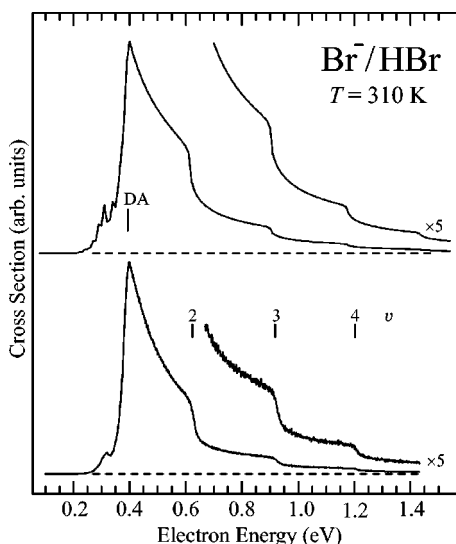


FIG. 12. Experimental (lower part) and theoretical (upper part) dissociative attachment cross sections in HBr at 310 K. The thresholds for dissociative attachment and vibrational excitation are marked. The theoretical spectrum is not convoluted with a simulated instrumental profile.

onset of the cross section at threshold in all other channels. The magnitude of the cross section is 5–25% smaller than in the previous calculation.

The situation is similar for vibrational excitation of DBr, shown in Fig. 15. The difference between the new and the old model is again small, with the exception of the fine structure in the  $v=0 \rightarrow 1$  channel and the threshold peak in the  $0 \rightarrow 2$  channel. The threshold peak in the  $0 \rightarrow 2$  cross section is smaller in the new model, and it is not clear whether it should be called a threshold peak at all. Note, however, that

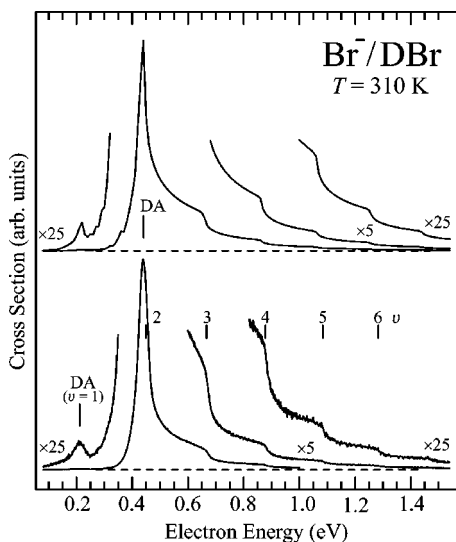


FIG. 13. Experimental (lower part) and theoretical (upper part) dissociative attachment cross sections in DBr at 310 K. The thresholds for vibrational excitation, dissociative attachment, and dissociative attachment to HBr in the  $v=1$  state are marked. The theoretical spectrum is not convoluted with a simulated instrumental profile.

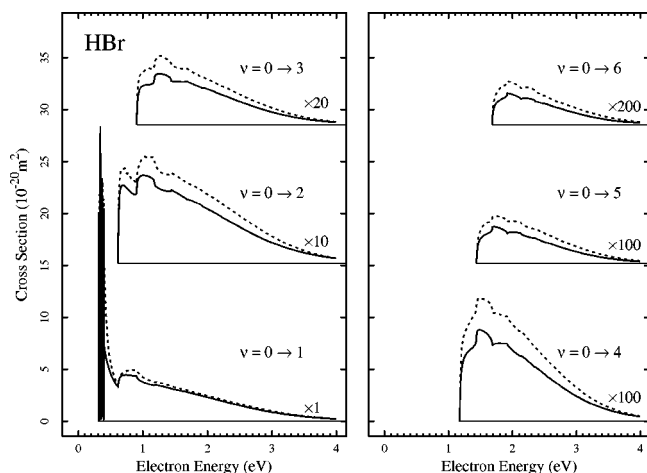


FIG. 14. Cross sections for vibrational excitation in HBr, shown in the same format as the measurement in Fig. 6. The dashed line shows the result of the previous model of Horáček and Domcke [17].

the peak is extremely close to the DA threshold, which renders the cross section extremely sensitive to small changes of the model parameters.

Let us now discuss the narrow structures in the  $v=0 \rightarrow 1$  vibrational excitation functions of HBr and DBr. These structures are very sensitive to the details of the HBr<sup>-</sup> potential at intermediate and large distances and were not as clearly developed in the previous model. We show details of the  $0 \rightarrow 1$  cross section for both HBr and DBr in Fig. 16, together with the resonant contribution to the elastic cross section. To clarify the relation of these structures with the HBr<sup>-</sup> potential, the energy of the bottom of the outer well in the ion potential is shown in the figure together with the DA threshold (dotted-vertical lines). These two energies define the borders of the region in which the sharp structures are present. There is another interesting feature of these structures. In the energy range where higher channels are closed, the cross section can drop to zero at each dip (see, for example, the HBr  $0 \rightarrow 0$  cross section in the region 0.25–0.315 eV), while in the energy range where at least one higher

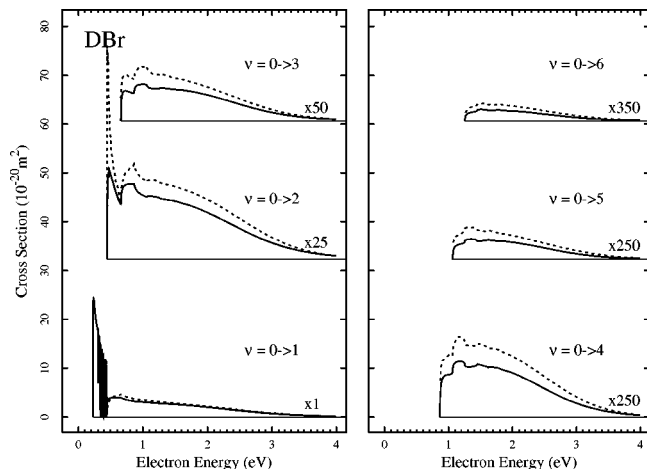


FIG. 15. The same as Fig. 14 for DBr.

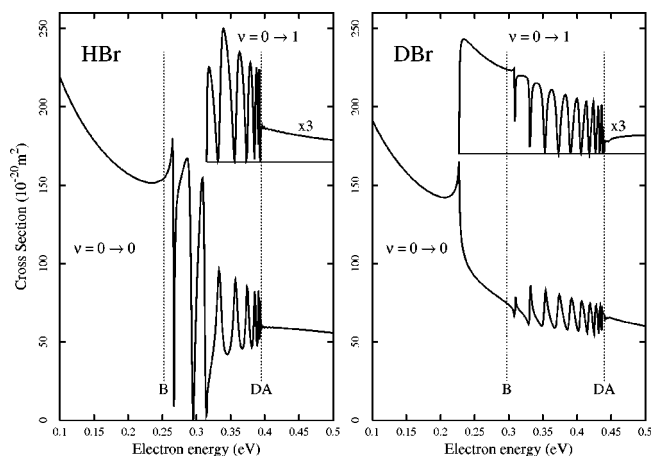


FIG. 16. Theoretical predictions of structures in the elastic and  $0 \rightarrow 1$  VE (shifted and magnified by factor of 3) cross sections for HBr and DBr. The dissociative attachment threshold and the bottom of the well in the ion potential (B) at  $R \sim 4a_0$  (see Fig. 5) are indicated.

channel is open, the amplitude of the structures is much smaller and the dips do not reach zero (see, for example, the HBr  $0 \rightarrow 0$  cross section above 0.315 eV). For both HBr and DBr the elastic cross section exhibits a pronounced cusp at the opening of the  $0 \rightarrow 1$  channel, although in the case of HBr it is hidden in the oscillatory structures.

The nature of these structures is very similar to those found previously in HCl [13,15]. The lowest, rather sharp, structures are window resonances associated with quasistationary levels of the outer well of the  $\text{HBr}^-$  potential-energy function. They can decay by tunneling through the barrier separating the outer well from the inner part of the potential-energy function, followed by autodetachment. With increasing energy, the outer-well resonances begin to overlap and develop into oscillatory structures, which are known as boomerang oscillations [11]. The boomerang oscillations converge towards the DA threshold, as has been observed also in  $e + \text{H}_2$  [47,48] and  $e + \text{HF}$  [10].

To complete the study of the low-energy collisions of electrons with HBr and DBr molecules, we have calculated the DA cross section. The cross sections for DA to the molecule in its first three vibrational states are shown in Fig. 17 in comparison with the previous calculation of Horáček and Domcke [17]. As in the case of vibrational excitation, the difference between the two calculations is small, except at the threshold. The enhancement of the cross section at the threshold in the present calculation can be attributed to the long-range polarization term  $-2.25R^{-4}$  of the discrete state potential  $V_d(R)$ . In the case of DBr, the DA cross sections at the threshold are further enhanced due to the vicinity of the Wigner cusp at the  $0 \rightarrow 1$  and  $0 \rightarrow 2$  vibrational excitation thresholds.

We have also calculated cross sections for DA to rotationally excited molecules. These cross sections are necessary for predictions of DA cross sections for hot molecules. Such cross sections were measured for HF and HCl by Allan and Wong [49]. Predictions of DA cross sections for hot HBr and DBr molecules are shown in Fig. 18. We have averaged the

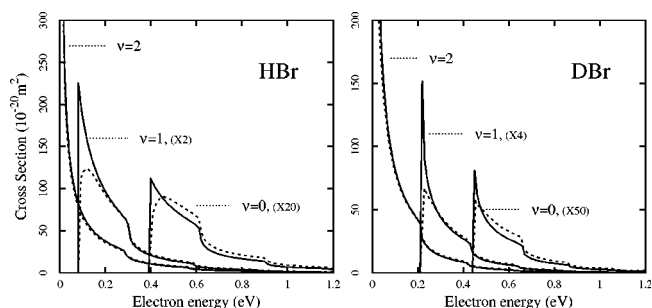


FIG. 17. Dissociative attachment to HBr (DBr) in specific vibrational states ( $J=0$ ). Results of the previous calculation of Horáček and Domcke [17] are shown as dashed lines.

cross sections for the attachment of electrons to rovibrationally excited molecules ( $v=0-3$ ,  $J=0-30$ ) over the Maxwell-Boltzmann distribution for two temperatures,  $T=500$  K and  $T=1000$  K (dotted lines). To simulate the finite resolution of the spectrometer, we have additionally convoluted the averaged cross section with a Gaussian function (FWHM 50 meV) (solid lines).

For both temperatures the cross sections exhibit steplike features (Wigner cusps) in the high-energy flank related to the opening of the  $0 \rightarrow 2$ ,  $0 \rightarrow 3$ , and  $0 \rightarrow 4$  VE channels. For energies below 0.5 eV we observe for HBr a peak for  $T=1000$  K and a shoulder for  $T=500$  K, which are due to molecules in the ground vibrational, but rotationally excited state,  $J \sim 10$ . Cross sections for this particular  $J$  are enhanced at threshold due to the Wigner cusp at the opening of the  $0 \rightarrow 1$  vibrational process. Another peak is present in HBr for  $T=1000$  K at low energies. This peak results mainly from DA to molecules in rovibrational states  $v=1$ ,  $J \geq 8$ . This peak is absent for  $T=500$  K, since the number of sufficiently excited molecules is too small. The interpretations of the structures for DBr is similar.

Overall, the temperature dependence of the DA cross section in HBr and DBr is similar (even somewhat more pronounced) as has been found experimentally [49] and theoretically [13] for HCl and DCl. The significant temperature dependence arises from the pronounced increase of the DA cross section for vibrationally and rotationally excited target molecules. It is conceivable that the high sensitivity of the HBr/DBr DA cross section to temperature could be exploited

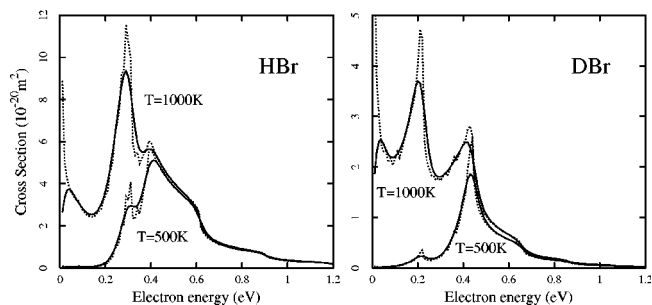


FIG. 18. Dissociative attachment to hot HBr and DBr molecules (dotted lines). The cross section convoluted with a Gaussian (FWHM 50 meV) to simulate the finite experimental resolution is shown as a solid line.

for *in situ* measurements of temperatures in gases and dilute plasmas.

## V. COMPARISON OF EXPERIMENT AND THEORY

In this section, we focus on the comparison of the shapes and relative magnitudes of the experimental differential cross sections with the theoretical cross sections described in the preceding section. The theory involves the simplifying assumption that only the  $s$  wave continuum contributes to resonant scattering and the calculated cross sections are integral cross sections. The dominance of the  $s$  wave is a reasonable assumption for low-energy scattering via a  $^2\Sigma$  shape resonance. We can thus compare the shapes of the experimental differential cross sections of Figs. 6 and 7 with the theoretical integral cross sections of Figs. 14 and 15. The comparison reveals that most of the qualitative predictions of the theory are confirmed by the experiment.

In particular, the experiment confirms the theoretical prediction that significant threshold peaks occur only in the  $v=0\rightarrow 1$  cross section of HBr, but in both the  $v=0\rightarrow 1$  and  $v=0\rightarrow 2$  cross sections of DBr. This confirms that threshold peaks are found in the excitation of those vibrational levels which lie below the DA threshold. The theoretical results are somewhat ambiguous concerning the threshold peak in the  $v=0\rightarrow 2$  channel of DBr. In the present calculation, this peak is less pronounced than in the previous [17] calculation. The experimental finding (Fig. 6) lies between the theoretical estimates.

There are differences between the experimental and theoretical excitation functions at the quantitative level. It is obvious that the broad shape resonance, which appears near 1.5–2.0 eV in the experimental VE cross sections, is located too low in the theoretical cross sections (near 1 eV). The location of the shape resonance in the theoretical model is determined by the *ab initio* phase shift of Fandreyer *et al.* [20]. The comparison with experiment indicates that the *ab initio* scattering calculation underestimates the  $^2\Sigma$  shape-resonance energy, presumably due to overcorrelation of the anion relative to the target.

A quantitative comparison of the calculated intensity ratio between the threshold peak and the maximum of the  $\sigma^*$  resonance with experiment is not considered useful, as the experimental determination of the intensity of the threshold peak is rather insecure, depending on details such as the energy resolution, the cutoff of the analyzer transmittivity at very low energies, and the uncertainty in the response function. For a more substantial quantitative comparison of experiment and theory, we consider the ratios of cross sections of different channels for an electron energy 0.1 eV above threshold. These data are given in Table III. It is seen that theory predicts the trends reliably for both HBr and DBr, the maximum deviation being a factor of 2 for small ratios. For the  $\sigma_{0\rightarrow v}/\sigma_{0\rightarrow v+1}$  ratios the deviation of theory from experiment is less than 30%.

Since the structures predicted in the elastic and  $0\rightarrow 1$  VE cross sections below the DA threshold are very narrow, it is necessary to take into account thermal rotational excitation of the target and the finite resolution of the spectrometer

TABLE III. Ratios of cross sections for vibrational excitation.

	HBr		DBr	
	Theory	Experiment	Theory	Experiment
$\sigma_{0\rightarrow 2}/\sigma_{0\rightarrow 1}$	0.19	0.26	0.15	0.15
$\sigma_{0\rightarrow 3}/\sigma_{0\rightarrow 1}$	0.053	0.096	0.036	0.059
$\sigma_{0\rightarrow 4}/\sigma_{0\rightarrow 1}$	0.018	0.030	0.011	0.023
$\sigma_{0\rightarrow 5}/\sigma_{0\rightarrow 1}$	0.007	0.012	0.004	0.010
$\sigma_{0\rightarrow 5}/\sigma_{0\rightarrow 1}$	0.003	0.005	0.002	0.006
$\sigma_{0\rightarrow 1}/\sigma_{0\rightarrow 2}$	5.3	3.8	6.7	6.5
$\sigma_{0\rightarrow 2}/\sigma_{0\rightarrow 3}$	3.6	2.8	4.1	2.6
$\sigma_{0\rightarrow 3}/\sigma_{0\rightarrow 4}$	3.0	3.2	3.2	2.5
$\sigma_{0\rightarrow 4}/\sigma_{0\rightarrow 5}$	2.7	2.4	2.7	2.3
$\sigma_{0\rightarrow 5}/\sigma_{0\rightarrow 6}$	2.3	2.6	2.4	1.7

before comparing calculation and experiment. We thus calculated the cross section for each vibrational excitation process for several values of the angular momentum  $J$  of the target molecule, and then performed the averaging of the cross section over the Maxwell-Boltzmann distribution of the rotational states for the assumed temperature of 100 K. This causes considerable broadening of the structures, since the narrow structures of the individual cross sections shift towards lower energies with increasing  $J$ . Furthermore, we convoluted the averaged cross section with a Gaussian of 5-meV FWHM to simulate the finite-energy resolution of the electron spectrometer. The convolution width was intentionally chosen narrower than the experimental resolution (about 15 meV) to preserve some of the finer details of the theoretical spectrum. These cross sections are compared with the experiment in Figs. 8–11.

Considering first the vibrationally elastic cross section in DBr, three features can be discerned in Fig. 9: a pronounced drop of the cross section at the  $v=1$  threshold, weak oscillatory boomerang structure in the 0.3–0.4 eV range, converging towards the DA threshold, and a weak change of the slope of the cross section at the  $v=2$  threshold. All three features are reproduced by theory. For the elastic cross section of HBr (Fig. 7), the boomerang oscillations are more pronounced. The step at the  $v=1$  threshold falls into the boomerang oscillations because of the closeness of the  $v=1$  and DA thresholds. The excellent quantitative agreement between experiment and theory for both HBr and DBr validates the theoretical model and confirms the high accuracy of the *ab initio* HBr<sup>-</sup> potential-energy function.

Excellent agreement between theory and experiments is also found for the structures of HBr and DBr in the  $v=0\rightarrow 1$  cross sections in Figs. 10 and 11. The upward and downward steps at the  $v=2$  and  $v=3$  thresholds are well reproduced.

The experiment resolves the oscillatory structures in HBr only marginally, in the form of a shoulder, because of the difficulty of the measurements very close to the threshold. The oscillatory structure is observed clearly in DBr, where the difference between the  $v=1$  and DA thresholds is large. The threshold peaks appear narrower and higher in the experiment than in the theory, in particular for DBr, but these

differences may be due to inaccuracies of the response function of the electrostatic instrument close to threshold. The results from the magnetically collimated spectrometer, shown in Figs. 6 and 7, are more reliable in this respect.

Finally, we compare the calculated and measured DA cross sections in Figs. 12 and 13. The pronounced Wigner cusps at the vibrational thresholds are predicted with high accuracy by the calculation. Theory and experiment agree that the cross section has the form of a narrow peak in DBr, caused by the fact that the cusp at the  $v=2$  threshold is only 10 meV above the DA threshold. The experiment confirms the prediction of the new model that the cross sections are sharply pointed and not rounded at threshold in HBr (see also Fig. 17). The small peak 75 meV below the DA threshold in the  $\text{Br}^-/\text{HBr}$  spectrum results from enhanced attachment to rotationally excited target molecules with  $J\sim 10$ , as discussed in Sec. IV B. The relative height of this hot band is less in the experiment ( $\sim 10\%$  of peak signal) than in the theory ( $\sim 20\%$ ). The difference could, however, be due to residual rotational cooling of the sample HBr, which was introduced through a 30- $\mu\text{m}$  nozzle, albeit with a low backing pressure (see Sec. II). The small peak 228 meV below the DA threshold in the  $\text{Br}^-/\text{DBr}$  spectrum results from enhanced attachment to vibrationally excited target molecules with  $v=1$ . The relative height of this hot band is the same in the experiment and in the theory ( $\sim 0.5\%$  of peak signal), indicating that the theoretical prediction of the cross section increase with vibrational excitation is quantitatively correct. Vibrational cooling in a gas expansion is much less efficient than rotational cooling and does not affect the comparison of theory and experiment. The relative height of the  $\text{Br}^-/\text{DBr}$  cross section in the 0.25–0.4 eV energy range, which is due to rotationally excited targets, is lower in the experiment than in the theory, presumably because of residual rotational cooling as in the case of HBr.

## VI. CONCLUSIONS

Recent experimental [4,10,15] and theoretical [8,13,22] results on low-energy electron collisions with HF and HCl, as well as the present results on the electron-HBr/DBr system, demonstrate that the hydrogen halides provide a much richer variety of resonance phenomena than the long-time prototype system  $\text{N}_2$ . In addition to the well-established shape resonance in HCl and HBr, threshold peaks in some VE channels, Wigner cusp structure in DA and VE cross sections and vibrational Feshbach resonances, it is now established that boomerang-type undulations of the cross sections and narrow interference structures due to outer-well resonances are common features in electron collisions with hydrogen halides.

With the completion of the experimental data for HBr (this paper) and HI [18], it is definitively established that threshold peaks exist only for the excitation of vibrational levels, which are energetically below the DA threshold. This finding confirms previous theoretical interpretations that associate threshold peaks with vibrational Feshbach reso-

nances, i.e., poles of the multichannel  $S$  matrix, which represent quasibound levels of the anion and are located below the vibrational levels of the target molecule [50,51].

The boomerang oscillations and the outer-well resonances are a very sensitive probe of the potential-energy function of the anion at intermediate and large internuclear distances. The ability to experimentally resolve these narrow structures has created a type of spectroscopy of anion potential-energy surfaces. As nicely illustrated by Figs. 10 and 11 for HBr and DBr, the threshold peaks act as a ‘‘magnifying glass,’’ enhancing the intensity of the narrow structures. Both in HCl [15] as well as in HBr/DBr (this paper), the calculated energies of the outer-well resonances agree with experiment within a few meV, demonstrating impressively the accuracy of the *ab initio* anion potential-energy function used as input to the models.

The molecular properties responsible for the richness of phenomena in low-energy electron scattering from hydrogen halides appear to be the dipole moment, the relatively large polarizability, and the low threshold for dissociative attachment. These properties are encountered widely in more complex molecules. The hydrogen halides are thus prototypes of a wide range of polyatomic targets, which accentuates the importance of a full understanding of the electron-scattering dynamics in hydrogen halides.

While the improved nonlocal resonance model for HBr constructed in the present paper has been found to reproduce all observed phenomena qualitatively correctly, some deficiencies in terms of quantitative accuracy remain. The location of the shape resonance is given too low by the *ab initio*  $R$ -matrix calculation of Fandreyer *et al.* [20], indicating slight overcorrelation of the anion relative to the target molecule. In the vicinity of the crossing region of the HBr and  $\text{HBr}^-$  potential-energy functions, both the electron-HBr scattering calculation [20] as well as the  $\text{HBr}^-$  bound-state calculation (this paper) become inaccurate owing to technical limitations. In the former case this arises from the incomplete inclusion of correlation effects associated with bond breaking in HBr, in the latter case primarily from the finite-basis representation of the extra electron and the inapplicability of the Ritz variational principle for electronic states in the continuum. These inaccuracies of the *ab initio* data affect, in particular, the height of the barrier that separates the dipole-bound inner part of the  $\text{HBr}^-$  potential-energy function from the outer well (cf. Fig. 5). The AD cross section at low collision energies, for example, depends very sensitively on the height of this barrier [13]. More accurate *ab initio* calculations in this critical and technically difficult range of the internuclear distance would be of great value.

## ACKNOWLEDGMENTS

This research has been supported by Project No. MŠMT KONTAKT ME273 and GACR 203/00/1025. This research is part of Project No. 20-53568.98 of the Swiss National Science Foundation.

- [1] K. Rohr and F. Linder, *J. Phys. B* **8**, L200 (1975).
- [2] K. Rohr and F. Linder, *J. Phys. B* **9**, 2521 (1976).
- [3] K. Rohr, *J. Phys. B* **11**, 1849 (1978).
- [4] S. Cvejanović, in *The Physics of Electronic and Atomic Collisions* 18th ICPEAC, Aarhus, edited by T. Andersen *et al.* (A.I.P., New York, 1993), p. 390.
- [5] M. A. Morrison, *Adv. At. Mol. Phys.* **24**, 51 (1988).
- [6] I. I. Fabrikant, *Comments At. Mol. Phys.* **24**, 37 (1990).
- [7] W. Domcke, *Phys. Rep.* **208**, 97 (1991).
- [8] J. Horáček, in *The Physics of Electronic and Atomic Collisions* XXI ICPEAC, Sendai, edited by Y. Itikawa *et al.* (A.I.P., New York, 1999), p. 329.
- [9] G. Knoth, M. Gote, M. Rädle, K. Jung, and H. Erhardt, *Phys. Rev. Lett.* **62**, 1735 (1989).
- [10] A.-Ch. Sergenton, L. Jungo, and M. Allan, *Phys. Rev. A* **61**, 062702 (2000).
- [11] A. Herzenberg, *J. Phys. B* **1**, 548 (1968).
- [12] W. Domcke and C. Mündel, *J. Phys. B* **18**, 4491 (1985).
- [13] M. Čížek, J. Horáček, and W. Domcke, *Phys. Rev. A* **60**, 2873 (1999).
- [14] O. Schafer and M. Allan, *J. Phys. B* **24**, 3069 (1991).
- [15] M. Allan, M. Čížek, J. Horáček, and W. Domcke, *J. Phys. B* **33**, L209 (2000).
- [16] R. Azria, Y. Le Coat, and J. P. Guillotin, *J. Phys. B* **13**, L505 (1980).
- [17] J. Horáček and W. Domcke, *Phys. Rev. A* **53**, 2262 (1996).
- [18] A.-Ch. Sergenton and M. Allan, *Chem. Phys. Lett.* **319**, 179 (2000).
- [19] J. Horáček, W. Domcke, and H. Nakamura, *Z. Phys. D: At., Mol. Clusters* **42**, 181 (1997).
- [20] R. Fandreyer, P. G. Burke, L. A. Morgan, and C. J. Gillan, *J. Phys. B* **26**, 2325 (1993).
- [21] H. Meyer, J. Horáček, and L. S. Cederbaum, *Phys. Rev. A* **43**, 3587 (1991).
- [22] J. Horáček, M. Čížek, and W. Domcke, *Theor. Chem. Acc.* **100**, 31 (1998).
- [23] M. Čížek, J. Horáček, and W. Domcke, *J. Phys. B* **31**, 2571 (1998).
- [24] M. Allan, *Helv. Chim. Acta* **65**, 2008 (1982).
- [25] M. Allan, *J. Electron Spectrosc. Relat. Phenom.* **48**, 219 (1989).
- [26] K. R. Asmis and M. Allan, *J. Phys. B* **30**, 1961 (1997).
- [27] A. Stamatović and G. J. Schulz, *Rev. Sci. Instrum.* **41**, 423 (1970).
- [28] M. Allan, *J. Phys. B* **25**, 1559 (1992).
- [29] M. Allan, *J. Phys. B* **28**, 5163 (1995).
- [30] M. Dolg, *Mol. Phys.* **88**, 1645 (1996).
- [31] W. Müller, J. Flesch, and W. Meyer, *J. Chem. Phys.* **80**, 3297 (1984); W. Müller and W. Meyer, *ibid.* **80**, 3311 (1984).
- [32] Y. Le Coat, R. Azria, and M. Tronc, *J. Phys. B* **15**, 1569 (1982).
- [33] MOLPRO is a package of *ab initio* programs written by H. J. Werner and P. J. Knowles; with contributions from J. Almlöf, R. D. Amos, M. J. O. Deegan, S. T. Elbert, C. Hampel, W. Meyer, K. Peterson, R. M. Pitzer, A. J. Stone, P. R. Taylor, H. J. Werner, and P. J. Knowles, *J. Chem. Phys.* **89**, 5803 (1988); P. J. Knowles and H. J. Werner, *Chem. Phys. Lett.* **145**, 514 (1988); H. J. Werner and P. J. Knowles, *Theor. Chim. Acta* **78**, 175 (1990); C. Hampel, K. Peterson, and H. J. Werner, *Chem. Phys. Lett.* **190**, 1 (1992).
- [34] P. G. Szalay and R. J. Bartlett, *Chem. Phys. Lett.* **214**, 481 (1993).
- [35] T. Leininger and F. X. Gadea, *J. Phys. B* **33**, 735 (2000).
- [36] H. Hotop and W. C. Lineberger, *J. Phys. Chem. Ref. Data* **14**, 731 (1985).
- [37] D. A. Chapman, K. Balasubramanian, and S. H. Lin, *Phys. Rev. A* **38**, 6098 (1988).
- [38] F. X. Gadea and I. Paidarova, *Chem. Phys.* **209**, 281 (1998).
- [39] K. P. Huber and G. Herzberg, *Molecular Spectra and Molecular Structure*, Vol. IV, Constants of Diatomic Molecules (Van Nostrand, New York, 1979).
- [40] S. V. O'Neil, P. Rosmus, D. W. Norcross, and H.-J. Werner, *J. Chem. Phys.* **85**, 7232 (1986).
- [41] P. Astrand and D. Karlström, *Chem. Phys. Lett.* **175**, 624 (1990).
- [42] H.-J. Werner and P. Rosmus, *J. Chem. Phys.* **73**, 2319 (1980).
- [43] R. J. Buenek, *Phys. Rev. A* **18**, 392 (1978).
- [44] J. F. Ogilvie, W. R. Dodwell, and R. H. Tipping, *J. Chem. Phys.* **73**, 5221 (1980).
- [45] R. Fandreyer and P. G. Burke, *J. Phys. B* **29**, 339 (1996).
- [46] S. Cvejanović and J. Jureta, *Abstract of the 3rd European Conference on Atomic and Molecular Physics Bordeaux, 1989*, p. 638.
- [47] M. Allan, *J. Phys. B* **18**, L451 (1985).
- [48] C. Mündel, M. Berman, and W. Domcke, *Phys. Rev. A* **32**, 181 (1985).
- [49] M. Allan and S. F. Wong, *J. Chem. Phys.* **74**, 1687 (1981).
- [50] J.-P. Gauyacq and A. Herzenberg, *Phys. Rev. A* **25**, 2959 (1982).
- [51] A. Schramm, I. I. Fabrikant, J. M. Weber, E. Leber, M. W. Ruf, and H. Hotop, *J. Phys. B* **32**, 2153 (1999).
- [52] M. Cizek, J. Horacek, F. A. U. Thiel, and H. Hotop, *J. Phys. B* (to be published).